

SNX

Swiss-Norwegian Foundation for Research with X-Rays

Report 2022

Contents

General Remarks.....	4
Introduction	5
ESRF highlight from SNBL.....	6
Developing synthesis-structure-activity relationships for Cu-mordenite systems.....	7
ESRF Spotlight from SNBL	9
Revealing the dynamics of active species in electrocatalysts under <i>operando</i> conditions.....	10
SNBL Scientific Highlights.....	12
Anatomy of a 2D Polymer Formation in the Single Crystal	12
Real-time regeneration of a working zeolite monitored via operando X-ray diffraction and crystallographic imaging: how coke flees the MFI framework	14
Scientific output Impact Factors	16
Scientific output Research Areas	17
Publication list 2022.....	18
SNBL software outreach	23
Summary of the works.....	24
BM01 installation of SAXS detector lift.....	24
BM31 installation of new end-station	24
Commissioning of the CdTe 2M detector	26
Benchmarking of X-ray total scattering and XAS data with the new endstation	27
Conclusions and outlook.....	29

General Remarks

The year 2022 is the nineteenth year of the SNX Foundation.

The accounting is supervised by OPTIMA COMPTA, in Seyssinet-Pariset, in Isère, for the two French associations, and by BfB Fidam Fiduciaire in Renens VD for the SNX Foundation. AUDICT FIDUCIAIRE in Lausanne audits the accounts.

These legal frameworks contribute to the smooth running of the collaborations and to the successful scientific work done at the Swiss Norwegian Beam Lines at ESRF.

The activities of the SNX Foundation are carried out at the European Synchrotron Radiation Facility (ESRF) in Grenoble and comprise the operation and up-grade of two beam line branches, called the Swiss-Norwegian Beam Lines (SNBL).

Introduction

This report covers the year 2022, the second of the 4-year contract (2021-2024) between the Swiss partner, the École Polytechnique Fédérale de Lausanne (EPFL) and for Norway the Norwegian University of Science and Technology (NTNU).

Obviously, the user program continued in 2022, moreover the phase 2 major upgrade program, spanning over the 4-year contract period, for SNBL is in full swing. This plan foresees that on BM01, Bragg diffraction, diffuse and small angle scattering, for single crystal, thin films and powder samples will become available. On BM31 it is planned that the combined diffraction and X-ray absorption experiments setup will be completed with Total Scattering and improvements in time and space resolution for all techniques. Improvements in beamline controls and online data analysis tools are also in the pipeline. The BM01 phase 2 upgrade has moderate cost. The BM31 phase 2 project however has a total investment budget of ~2 Million Euro's. Where 2021 was very much a development and investment year. 2022 was marked by a massive assembly, testing, installation and implementation works on especially the BM31 beamline while running practically a full user program. Only 7 days were taken out of the available beamtime for users despite a total renewal of the end-station. Overall the works and output can be summarized as follows:

1. A full user program was successfully and reliably executed on both beamlines.
2. 77 publications using SNBL data appeared in peer review journals, 19.5% of SNBL publications has an impact factor above 10 and 62% above impact factor 4.
3. In the summer shutdown the BM31 experimental hutch has been completely rebuild and tested.
4. On BM01 the SAXS detector setup was installed.

ESRF highlight from SNBL



Developing synthesis-structure-activity relationships for Cu-mordenite systems

The synthesis of materials such as copper zeolites for methane-to-methanol oxidation is influenced to a large degree by the nature of its constituents. X-ray absorption spectroscopy revealed that different Al sources influence the location of Al incorporation in the zeolite system, resulting in a Cu-zeolite system of varying propensity towards the selective oxidation of methane to methanol.

To mitigate the release of large amounts of methane and other small alkanes, the challenge of activating the strong C-H bond of these molecules needs to be addressed. While facilitated on a large scale in steam reforming facilities, Cu-zeolites show promise to provide a pathway towards more decentralised point-source mitigation strategies. Using inexpensive molecular oxygen to form active sites, Cu-zeolites can readily activate the C-H bond. Hereby, the methane molecule forms a methoxy intermediate and is subsequently extracted in the presence of water, yielding methanol. Among the various Cu-zeolites studied, Cu-mordenite exhibits the highest methanol productivity to date and various research has investigated the properties of this specific zeolite.

This work reports the successful use of different Al sources, namely aluminum sulfate and sodium aluminate, to crystallise a material that is in both cases mordenite zeolites – MOR-Al₂(SO₄)₃ and MOR-NaAlO₂ respectively – but that show distinct differences in the crystal morphology as well as the acid site distribution. Several techniques were used to investigate the Brønsted acidity of the material. Propylamine temperature-programmed desorption showcased that MOR-Al₂(SO₄)₃ has more acid sites compared to MOR-NaAlO₂, however, when using a smaller probe molecule such as NH₃, the same number of acid sites is obtained. Additional techniques such as titration of acid sites with CO followed by infrared spectroscopy, as well as using deuterated acetonitrile in combination with solid-state ¹H NMR present a similar trend (Figure 1).

These results suggest differences in the location of acid sites, with MOR-NaAlO₂ containing more acid sites in constrained spaces, such as the 8-ring side pocket, less accessible to larger molecules (e.g. propylamine). It was found that this Al distribution is influenced by the pH of the gel with a more alkaline gel (MOR-NaAlO₂) crystallising faster and likely incorporating Al in different locations compared to the slightly less alkaline gel of MOR-Al₂(SO₄)₃. Subsequently, Cu-mordenite samples were prepared based on these two archetype materials and it was found that the performance in the methane-to-methanol reaction varies amongst them; the MOR-Al₂(SO₄)₃ giving a higher methanol productivity compared to the MOR-NaAlO₂ sample. This, for the first time, showed that for the same material, a different propensity could be imparted in activating the C-H bond of methane.

Previous work focused on studying the active Cu species in mordenite using synchrotron radiation at the SNBL beamline, BM31 [1]. Analysing the X-ray absorption near-edge structure (XANES) spectra of the Cu k-edge, it was found that Cu-mordenite materials with exceptionally high productivity had a significant concentration of framework-associated Cu²⁺ species that are resistant to self-reduction, establishing a clear correlation between these species and the MeOH productivity across a range of Cu-Mordenite zeolites. Current work once more took advantage of BM31's capabilities and the XANES and extended X-ray absorption fine structure

(EXAFS) region of the Cu k-edge were collected for the select samples of the MOR- $\text{Al}_2(\text{SO}_4)_3$ and MOR- NaAlO_2 series. Figure 2 shows that the most productive sample (0.11CuHMOR- $\text{Al}_2(\text{SO}_4)_3$) also has the most intense white line in the XANES region as well as the largest first shell contribution in the EXAFS part.

Based on previous work, this suggests a larger concentration of the highly active Cu^{2+} species, indicating that the location of Al in the framework plays an important part in generating the most active species for the oxidation of methane to methanol. Thus, for the first time, a clear synthesis-structure-activity relationship is established for Cu-mordenite.

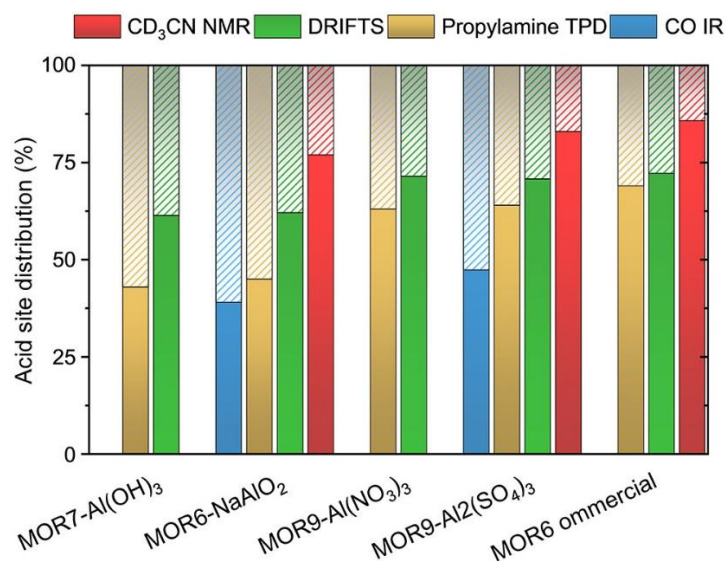


Fig. 1: Acid site distributions for MOR zeolites discussed in this study as assessed with several different techniques. Colour-coding is used to illustrate the respective techniques. The solid bars correspond to acid sites in the 12-ring (Al) with those in 8-rings making up the difference (patterned bars).

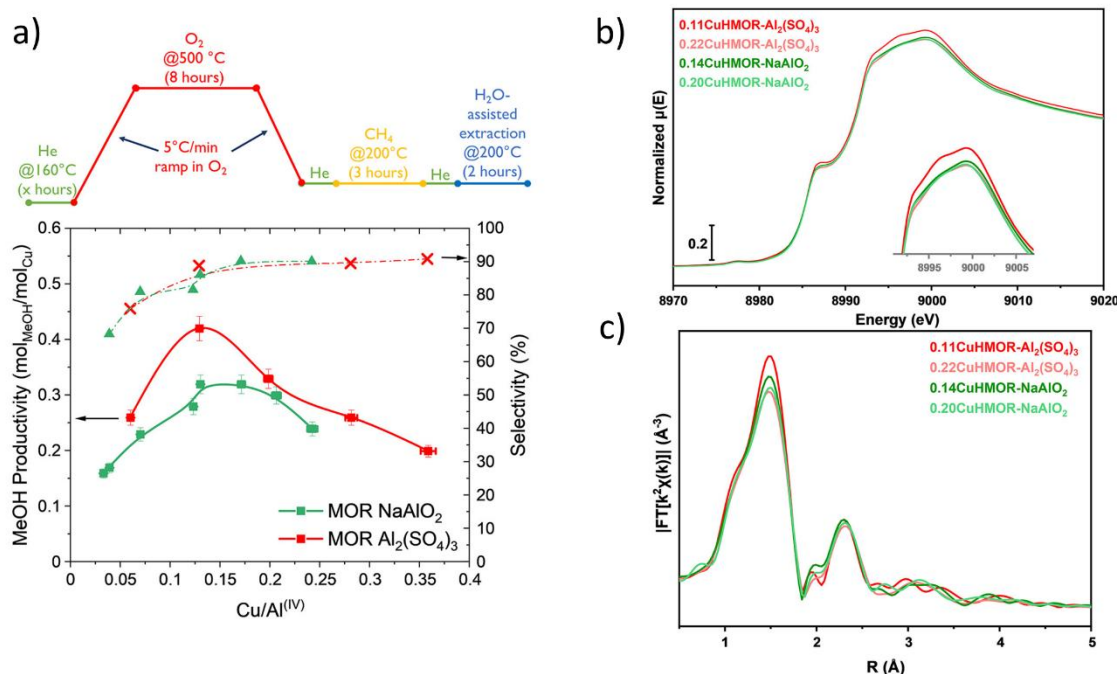


Fig. 2: a) Reaction protocol for partial oxidation of CH₄ and the MeOH productivity for the two mordenite (MOR) series. b) XANES spectra of the Cu K-edge for several activated Cu-mordenite samples previously synthesised and tested for the partial oxidation of CH₄. c) EXAFS region highlighting the first shell interactions.

Principal publication and authors

Synthesis–Structure–Activity Relationship in Cu-MOR for Partial Methane Oxidation: Al Siting via Inorganic Structure-Directing Agents, S. Prodingler (a), K. Kvande (a), B. Arstad (b), E. Borfecchia (c), P. Beato (d), S. Svelle (a), *ACS Catal.* **12**, 4, 2166-2177 (2022); <https://doi.org/10.1021/acscatal.1c05091>.

(a) Department of Chemistry, University of Oslo, (Norway)

(b) SINTEF Industry (Norway)

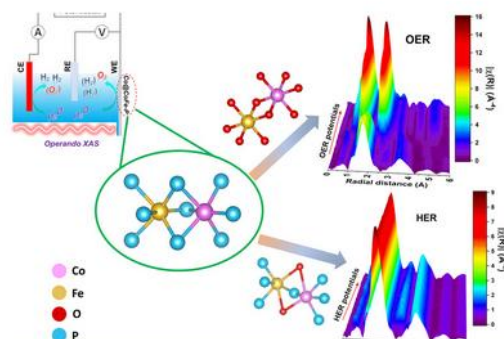
(c) Department of Chemistry, University of Turin (Italy)

(d) Haldor Topsøe A/S, (Denmark)

References

[1] D.K. Pappas *et al.*, *J. Am. Chem. Soc.* **140**, 15270 (2018).

ESRF Spotlight from SNBL



27-06-2022

Revealing the
dynamics of active
species in
electrocatalysts
under operando
conditions

→ Read more

Revealing the dynamics of active species in electrocatalysts under *operando* conditions

X-ray absorption spectroscopy at beamline BM31 was used to investigate the dynamics of true active species in cobalt phosphide/chalcogenide-based electrocatalysts under reaction conditions. The results offer new insights that could lead to the design of higher-performing catalysts to produce green hydrogen fuel.

The design of efficient electrocatalysts for industrial water splitting (i.e., separating H₂O into oxygen and hydrogen) is essential to generate sustainable hydrogen fuel. However, a comprehensive understanding of the complex catalytic mechanisms under harsh reaction conditions remains a major challenge. Over the past decades, several types of electrocatalysts have been designed for large-scale and low-cost hydrogen production. Among these, transition metal chalcogenides (TMCs) and phosphides (TMPs) show remarkable catalytic performance for both the hydrogen and oxygen evolution reactions ((HER and OER respectively), thus emerging as excellent candidates for practical alkaline exchange membrane (AEM) electrolyser systems [1].

Nevertheless, TMCs and TMPs undergo structural reconstructions during the reaction process, which renders the identification of their real catalytically active phases extremely difficult. Previous studies have shown strong correlation between the local electronic structure of the materials and their catalytic activity [2]. It is likely that the main phenomenon behind the excellent activity of TMCs/TMPs catalysts for OER is structural reconstruction into metal oxides/(oxy)hydroxides [3], although it is still unknown whether these are the real active phases for OER. In addition, whether the catalysts can also undergo structural reconstructions during HER still requires in-depth investigation. Recent advances in *in-situ/operando* techniques have established new routes to understanding catalytic structure-activity relationships on an atomic-resolution scale for guidance in the design of high-performance electrocatalysts [4].

The catalytic mechanisms of TMC and TMP was studied using *operando* Raman spectroscopy and X-ray absorption spectroscopy (XAS) at beamline BM31 to track the dynamics of true active species in cobalt phosphide/chalcogenide-based electrocatalysts under *operando* reaction conditions and to reveal the real catalytically active intermediates during water splitting. XAS tests were carried out with two representative samples for HER and OER, namely cobalt phosphides (referred to as Co-P material) and Co-P with partial Fe substitution (referred to as Co@CoFe-P material).

Figure 1 illustrates *operando* XAS characterisations of Co-P under *operando* HER conditions. For the HER, the rising absorption edge energy position of the *operando* Co K-edge XANES spectra featured a negative energy shift, indicating the formation of low-valent Co ions during the HER process (Figure 1a,b). Close inspection of the *operando* Co K-edge FT-EXAFS spectra (Figure 1c) revealed that the backscattering of the first coordination shells arising from Co-P pairs underwent peak profile changes during the HER. Further, after removal of the applied potential, a prominent backscattering peak in the second coordination shell arising from Co-Co pairs (present in Co-O-Co moieties) was observed in the *operando* FT-EXAFS spectra. This suggests that an oxidised form of Co-P featuring P-Co-O structural moieties comprising low-valent Co⁰/Co⁺ species performed as active HER catalyst.

In sharp contrast, *operando* XAS characterisations of Co-P during OER pointed to a series of dynamic structural transformations: Co-P → Co-P_{6-x}O_x → Co-P_{6-x}O_x@Co(OH)₂@CoOOH → Co-P_{6-x}O_x@Co(OH)₂ (transient)@CoOOH

→ CoOOH → CoO₂, where the *in-situ* reconstructed CoO₂ species with high-valent Co⁴⁺ centres served as the true OER active phases.

Additionally, *operando* XAS experiments with Co@CoFe-P for HER and OER were carried out to reveal the influence of secondary metal substitution on the electrochemical properties. This is a promising approach to improve both the catalytic activity and stability of catalysts with a single metal type. Similar to the *operando* XANES characterisation of Co-P during HER (Figure 1a,b), the *operando* Co K-edge XANES spectra of Co@CoFe-P (Figure 2a,b) also demonstrates the reduction of Co centres to a low-valence state. Analysis of *operando* Co-K edge FT-EXAFS spectra (Figure 2c) suggested that the *in-situ* reconstructed P-Co-O-Fe-P structural moieties played a key role during the *operando* HER tests.

In conclusion, synchrotron X-ray spectroscopy can be used to track the dynamics of the local coordination environments of metal centres and also to capture the key reactive intermediates during the electrolysis process. Such investigations will hold the key to deciphering the intrinsic catalytic mechanisms of important heterogeneous catalysts as a step towards improving technical electrolyzers and other areas of green hydrogen production.

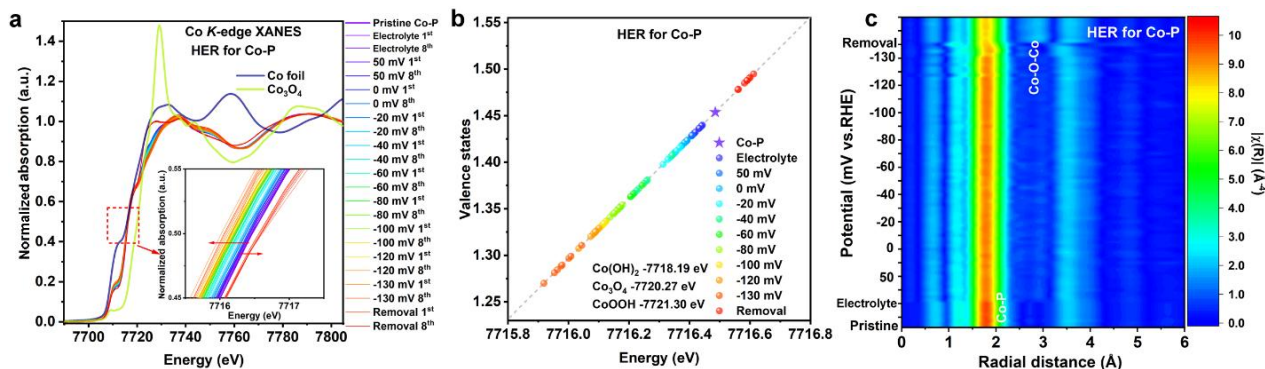


Fig. 1: *Operando* XAS characterisations of Co-P for HER. a) *Operando* Co K-edge XANES spectra of Co-P during HER. b) Calculated Co valence state vs. energy positions. c) 2D contour plots of Co K-edge FT-EXAFS spectra of Co-P during HER. Reproduced with permission from *Energy Environ. Sci.* 15, 727-739 (2022).

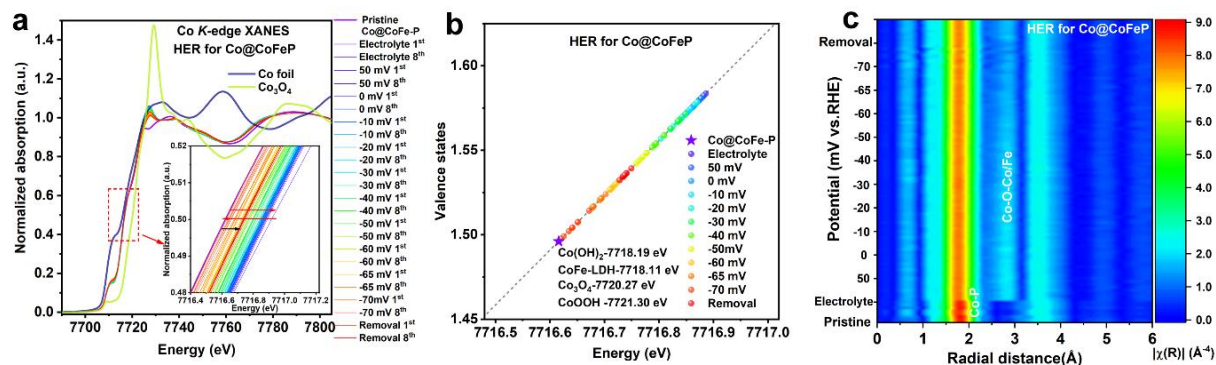


Fig. 2: *Operando* XAS characterisations of Co@CoFe-P for HER. a) *Operando* Co K-edge XANES spectra of Co@CoFe-P during HER. b) Calculated Co valence state vs. energy positions. c) 2D contour plots of Co K-edge FT-EXAFS spectra of Co@CoFe-P during HER.

FT-EXAFS spectra of Co@CoFe-P during HER. Reproduced with permission from *Energy Environ. Sci.* 15, 727-739 (2022).

Principal publication and authors

Dynamics and control of active sites in hierarchically nanostructured cobalt phosphide/chalcogenide-based electrocatalysts for water splitting, Y. Zhao (a), N. Dongfang (a), C.A. Triana (a), C. Huang (a), R. Erni (b), W. Wan (a), J. Li (a), D. Stoian (c), L. Pan (d), P. Zhang (e), J. Lan (a), M. Iannuzzi (a), G.R. Patzke (a), *Energy Environ. Sci.* **15**, 727-739 (2022); <http://www.doi.org/10.1039/D1EE02249K>

(a) Department of Chemistry, University of Zurich, Zurich (Switzerland)

(b) Electron Microscopy Center, Empa, Swiss Federal Laboratories for Materials Science and Technology, Dübendorf (Switzerland)

(c) Swiss-Norwegian Beamlines at the ESRF, Grenoble (France)

(d) Key Laboratory of Advanced Metallic Materials of Jiangsu Province, School of Materials Science and Engineering, Southeast University, Nanjing (China)

(e) School of Electrical and Information Engineering and Key Laboratory of Advanced Ceramics and Machining Technology of Ministry of Education, Tianjin University, Tianjin (China)

References

- [1] D. Li *et al.*, *Nat. Energy* **5**, 378-385 (2020).
- [2] Z.W. She *et al.*, *Science* **355**(6321), eaad4998 (2017).
- [3] H. Ding *et al.*, *Chem. Rev.* **121**(21), 13174-13212 (2021).
- [4] J. Timoshenko *et al.*, *Chem. Rev.* **121**(2), 882-961 (2021).

SNBL Scientific Highlights

Two works based on data from BM01 have been selected for the SNBL Highlights 2022. Both of them focus on exploring one of the last remaining white spots in structural science, which is the detailed understanding of the local structure. First paper is based on single crystal diffraction, diffuse scattering, and 3D- Δ PDF analysis, while the second deals with operando time-resolved powder diffraction coupled with mass spectroscopy, accurate structural analysis, and Fourier mapping of the residual electron density.

Anatomy of a 2D Polymer Formation in the Single Crystal

This work addresses the anatomy of a 2D polymer formation; that is, we identify, localize, and describe the various processes required to obtain such a macromolecule in a single-crystal-to-single-crystal reaction. It contains aspects of lattice, local and integral strain, and the distribution of strain in the crystal and assembles the various bits and pieces to a full-scale mechanistic picture providing experimental evidence for why the polymerization avoids phase segregation and why the crystals do not shatter as a result. While lattice strain is investigated by Bragg scattering, most of the paper revolves around diffuse scattering and its analysis with the three-dimensional difference pair distribution function (3D- Δ PDF). Finally, and more generally, this work shows that the 3D- Δ PDF method can treat highly complex disorder problems in depth. The fact that the analysis of the diffuse scattering has successfully been accomplished for this highly complex disorder problem

nevertheless reflects the power of the 3D- Δ PDF method in terms of achieving a self-consistent, molecular-scale mechanistic description of the strain management during polymerization and its impact on the results.

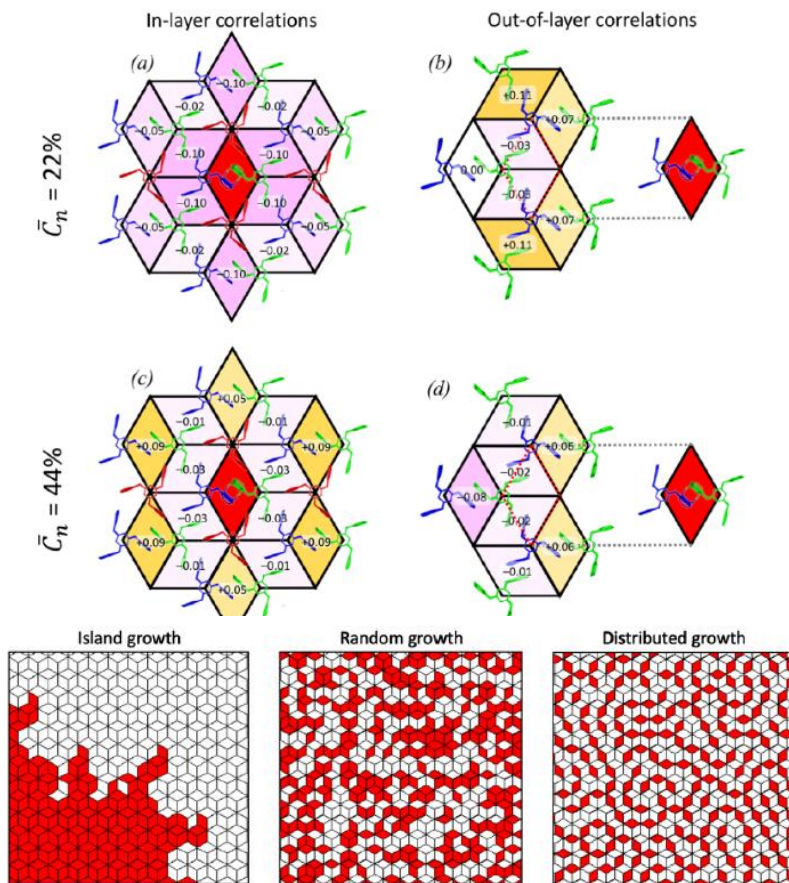


Figure. (top) Concept drawings of self-stimulating (strong positive correlation; left), random (zero correlation; middle), and self-impeding polymeric growth (strong negative correlation; right). (bottom) Substitutional correlations for (a) in-layer and (b) out-of-layer at conversion ratios of 22% and for (c) in-layer and (d) out-of-layer at a conversion ratio of 44%. In (b) and (d), the isolated rhomb indicates that dimerization occurred in the layer below, and dotted lines show the structural relation of that dimer with respect to the layer. Yellow rhombs refer to positive correlations and violet rhombs to negative correlations, while shadings and numbers within the rhombs indicate the strength of the correlation.

Principal publication and authors

Anatomy of a 2D Polymer Formation in the Single Crystal. In *Macromolecules*, 55(2), 568–583. DOI: 10.1021/acs.macromol.1c02189

Authors: Gregor Hofer^{1,2}, A. Dieter Schlüter², and Thomas Weber¹

Affiliations: ¹ X-ray Platform D-MATL, Department of Materials, ETH Zürich, Vladimir-Prelog-Weg 5-10, 8093 Zurich, Switzerland, ² Laboratory of Polymer Chemistry, Department of Materials, ETH Zürich, Vladimir-Prelog-Weg 5-10, 8093 Zurich, Switzerland

Real-time regeneration of a working zeolite monitored via operando X-ray diffraction and crystallographic imaging: how coke flees the MFI framework

A regeneration of H-ZSM-5 was monitored the regeneration of H-ZSM-5 via operando time-resolved powder X-Ray diffraction coupled with mass spectroscopy. By combining parametric Rietveld refinements and calculation of the extra-framework electronic density by difference Fourier maps analysis, we could reveal the evolution of the coke species, monitor the regeneration of the catalyst, and study the geometrical response of different framework domains as the solid coke species combust and abandon their preferential residing sites. A small amount of adsorbed molecular species and alkyl side chains are leaving the zeolite pores first, followed by the actual oxidation products of the majority of the coke. It is clear that the coke removal is a complex process that occurs in at least two steps; a thermal decomposition followed by oxidation. In a coked zeolite, the straight 10-ring channel circumference is warped to an oval shape due to structural distortion induced by rigid aromatic coke species. The data presented explain why the difference in length between the a-vector and the b-vector of the MFI unit cell is a robust descriptor for bulky coke, as opposed to the unit cell volume, which is affected also by adsorbed species and thermal effects. This work reveals the powerful nature of crystallographic analysis, that combined with the advances on data collection and processing can allow identification of specific coke locations within a three-dimensional zeolite framework and provide new insight into the industrially highly important regeneration step in the Methanol to Gasoline process.

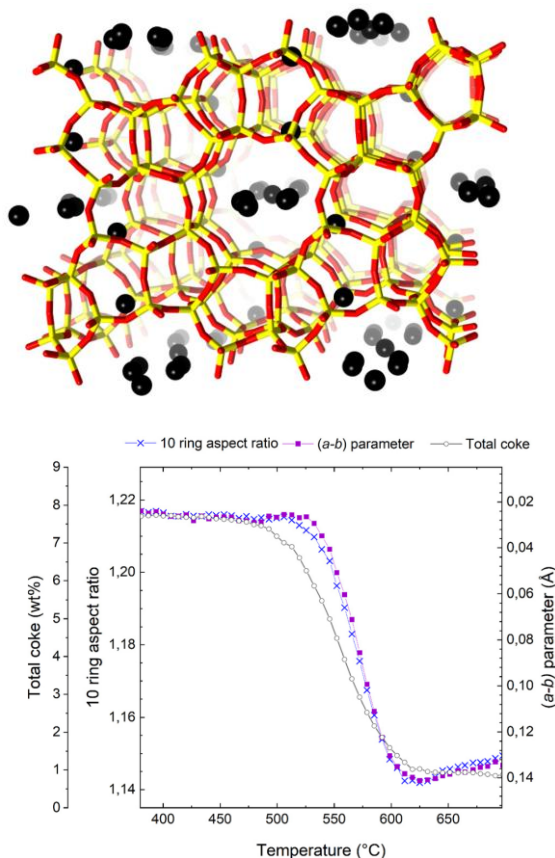


Figure. (top) H-ZSM-5 unit cell viewed along the b-axis. Framework oxygen atoms and T-atoms are indicated in red and yellow, respectively. Black spheres indicate preferential sites of coke residing in the framework. The coke sites have been identified by difference Fourier map analysis. (bottom) Total coke content from dummy atom occupancies (connected grey open circles), evolution of the (a - b) parameter (connected purple squares, note that the scale is inverted relative to Fig. 2), and 10 ring aspect ratio (connected blue crosses) during the course of regeneration of the H-ZSM-5 catalyst.

Principal publication and authors

Real-time regeneration of a working zeolite monitored via operando X-ray diffraction and crystallographic imaging: how coke flees the MFI framework *Dalton Trans.*, **2022**, 51, 16845, DOI: 10.1039/d2dt02845j

Authors: Georgios N. Kalantzopoulos¹, Daniel Rojo Gama¹, Dimitrios K. Pappas¹, Iurii Dovgaliuk^{3,4}, Unni Olsbye¹, Pablo Beato², Lars F. Lundegaard², David S. Wragg¹ and Stian Svelle¹

Affiliations : ¹ Center for Materials Science and Nanotechnology (SMN), Department of Chemistry, University of Oslo, P.O. Box 1033, BlindernN-0315 Oslo, Norway. ² Haldor Topsøe A/S, Haldor Topsøes Allé 1, 2800 Kgs Lyngby, Denmark. ³ Swiss-Norwegian Beamline at the European Synchrotron Facility, 71 avenue des Martyrs, F-38000 Grenoble, France. ⁴ Institut des Matériaux Poreux de Paris, Département de Chimie, ENS - UMR 8004 CNRS-ENS-ESPCI, 24 rue Lhomond, 75005 Paris, France.

Scientific output Impact Factors

77 peer reviewed papers were published in 2022 containing data from SNBL. 19.5% of the SNBL publications are published in journals with an impact factor above 10 and 62% above impact factor 4. See below the top part of the distribution of papers per journal in 2022 and their impact factor.

Journal	Impact Factor	Publications in 2022
ENERGY & ENVIRONMENTAL SCIENCE	39.714	1
TRENDS IN CHEMISTRY	22.448	1
ADVANCED FUNCTIONAL MATERIALS	19.924	1
ACS NANO	18.027	1
ANGEWANDTE CHEMIE-INTERNATIONAL EDITION	16.823	1
CHEMICAL ENGINEERING JOURNAL	16.744	1
JOURNAL OF THE AMERICAN CHEMICAL SOCIETY	16.383	2
JOURNAL OF MATERIALS CHEMISTRY A	14.511	1
ACS CATALYSIS	13.7	1
SCIENCE OF THE TOTAL ENVIRONMENT	10.754	1
CHEMISTRY OF MATERIALS	10.508	3
ACS APPLIED MATERIALS & INTERFACES	10.383	1
CHEMICAL SCIENCE	9.969	1
NANOSCALE	8.307	1
JOURNAL OF CATALYSIS	8.047	2
INTERNATIONAL JOURNAL OF HYDROGEN ENERGY	7.139	1
CATALYSIS TODAY	6.562	2
JOURNAL OF ALLOYS AND COMPOUNDS	6.371	1
CATALYSIS SCIENCE & TECHNOLOGY	6.177	3
CHEMICAL COMMUNICATIONS	6.065	1
MACROMOLECULES	6.057	1
APPLIED CATALYSIS A-GENERAL	5.723	1
NANOMATERIALS	5.719	1
CHEMCATCHEM	5.501	1
INORGANIC CHEMISTRY	5.436	4
JOURNAL OF MATERIALS SCIENCE	4.682	1
DALTON TRANSACTIONS	4.569	6
CATALYSTS	4.501	2
JOURNAL OF PHYSICAL CHEMISTRY C	4.177	3
CRYSTAL GROWTH & DESIGN	4.01	1
CRYSTENGGCOMM	3.756	1
JOURNAL OF SOLID STATE CHEMISTRY	3.656	1
ACS EARTH AND SPACE CHEMISTRY	3.556	1
CHEMPHYSICHEM	3.52	1
ENERGIES	3.252	1

Scientific output Research Areas

All the SNBL papers in 2022 were also classified by research area. As the earlier years it's clear SNBL has a strong portfolio in chemistry and materials science followed by physics and crystallography. See below the full distribution per Research Area.

Research Area	Number of Publications
CHEMISTRY, PHYSICAL	25
CHEMISTRY, MULTIDISCIPLINARY	21
MATERIALS SCIENCE, MULTIDISCIPLINARY	16
CHEMISTRY, INORGANIC & NUCLEAR	12
CRYSTALLOGRAPHY	12
NANOSCIENCE & NANOTECHNOLOGY	8
ENGINEERING, CHEMICAL	6
PHYSICS, APPLIED	5
ENERGY & FUELS	4
ENVIRONMENTAL SCIENCES	3
CHEMISTRY, APPLIED	2
ELECTROCHEMISTRY	1
ENGINEERING, ELECTRICAL & ELECTRONIC	1
ENGINEERING, ENVIRONMENTAL	1
GEOCHEMISTRY & GEOPHYSICS	1
INSTRUMENTS & INSTRUMENTATION	1
MATERIALS SCIENCE, CERAMICS	1
METALLURGY & METALLURGICAL ENGINEERING	1
OPTICS	1
PHYSICS, ATOMIC, MOLECULAR & CHEMICAL	1
PHYSICS, CONDENSED MATTER	1
PHYSICS, MULTIDISCIPLINARY	1
POLYMER SCIENCE	1

Publication list 2022

1. Ali, D., Li, Z., Azim, M.M., Lein, H.L., Mathisen, K. *Pinpointing basic sites formed upon incorporation of iron in hierarchical SAPO-11 using catalytic model reactions* Dalton Trans., 51, 15251-15262, 2022
2. Aree, T., McMonagle, C.J., Michalchuk, A.A.L., Chernyshov, D. *Low-frequency lattice vibrations from atomic displacement parameters of α -FOX-7, a high energy density material* Acta. Cryst., B78, 376-384, 2022
3. Bakken, K., Blichfeld, A.B., Nylund, I.-E., Chernyshov, D., Glaum, J., Grande, T., Einarsrud, M.-A. *Tailoring Preferential Orientation in BaTiO₃-based Thin Films from Aqueous Chemical Solution Deposition* Chem. Methods, 2, e202100064, 2022
4. Bakken, K., Grendal, O.G., Einarsrud, M.A. *In situ characterisation for studying nucleation and growth of nanostructured materials and thin films during liquid-based synthesis* J. Sol-Gel Sci Technol 105, 596-605, 2022
5. Balaghi, S.E., Heidari, S., Benamara, M., Beyzavi, H., Patzke, G.R. *Fluoride etched Ni-based electrodes as economic oxygen evolution electrocatalysts* International J. of Hydrogen Energy, 47, 1613-1623, 2022
6. Baral, P.R., Ukleev, V., LaGrange, T., Cubitt, R., Živković, I., Rønnow, H.M., White, J.S., Magrez, A. *Tuning Topological Spin Textures in Size-Tailored Chiral Magnet Insulator Particles* J. Phys. Chem. C, 126, 28, 11855-11866, 2022
7. Beck, A., Rzepka, P., Marshall, K.P., Stoian, D., Willinger, M.G., van Bokhoven, J.A. *Hydrogen interaction with oxide supports in the presence and absence of platinum* J. Phys. Chem. C, 126, 41, 17589-17597, 2022
8. Boytsova, O., Zhukova, I., Tatarenko, A., Shatalova, T., Beiltiukov, A., Eliseev, A., Sadovnikov, A. *The Anatase-to-Rutile Phase Transition in Highly Oriented Nanoparticles Array of Titania with Photocatalytic Response Changes* Nanomaterials, 12, 24, 4418, 2022
9. Brighi, M., Murgia, F., Lodziana, Z., Cerny, R. *Structural Phase Transitions in closo-Dicarbododecaboranes C₂B₁₀H₁₂* Inorg. Chem., 2022
10. Burazer, S., Horak, L., Filinchuk, Y., Cerny, R., Popovic, J. *Abrupt change from moderate positive to colossal negative thermal expansion caused by imidazolate composite formation* J. Mater. Sci., 57, 11563-11581, 2022
11. Castro-Fernández, P., Mance, D., Liu, C., Abdala, P.M., Willinger, E., Rossinelli, A.A., Serykh, A.I., Pidko, E.A., Copéret, C., Fedorov, A., Müller, C.R. *Bulk and surface transformations of Ga₂O₃ nanoparticle catalysts for propane dehydrogenation induced by a H₂ treatment* J. of Catalysis, 408, 155-164, 2022
12. Castro-Fernández, P., Serykh, A.I., Yakimov, A.V., Prosvirin, I.P., Bukhtiyarov, A.V., Abdala, P.M., Copéret, C., Fedorov, A., Müller, C.R. *Atomic-scale changes of silica-supported catalysts with nanocrystalline or amorphous gallia phases: implications of hydrogen pretreatment on their selectivity for propane dehydrogenation* Catal. Sci. Technol., 12, 3957-3968, 2022
13. Chardon, W.J., Groenenberg, J.E., Vink, J.P.M., Voegelín, A., Koopmans, G.F. *Use of iron-coated sand for removing soluble phosphorus from drainage water* Science of the Total Environment, 815, 152738, 2022
14. Chen, Z., Docherty, S.R., Florian, P., Kierzkowska, A., Moroz, I.B., Abdala, P.M., Copéret, C., Müller, C.R., Fedorov, A. *From ethene to propene (ETP) on tailored silica-alumina supports with isolated Ni(II)*

- sites: uncovering the importance of surface nickel aluminates sites and the carbon-pool mechanism Catal. Sci. Technol., 12, 5861-5868, 2022
15. Cherednichenko, K.A., Mukhanov, V.A., Kalinko, A., Solozhenko, V.L. *High-pressure synthesis of boron-rich chalcogenides B12S and B12Se* J. of Alloys and Compounds, 898, 162874, 2022
 16. Chernyshov, D., Dyadkin, V., Törnroos, K.W. *Preliminary observations of the interplay of radiation damage with spin crossover* Acta. Cryst., B78, 392-396, 2022
 17. Chi, H.-Y., Chen, C., Zhao, K., Villalobos, L.F., Schouwink, P.A., Piveteau, L., Marshall, K.P., Liu, Q., Han, Y., Agrawal, K.V. *Unblocking ion-occluded pore channels in Poly(triazine imide) framework for proton conduction* Angew. Chem.Int., 61, e202207457, 2022
 18. Cölfen, H., Bürgi, H.-B., Chernyshov, D., Stekiel, M., Chumakova, A., Bosak, A., Wehinger, B., Winkler, B. *Mesocrystalline structure and mechanical properties of biogenic calcite from sea urchin spine* Acta. Cryst., B78, 356-358, 2022
 19. Cornia, A., Nicolini, A., McMonagle, C.J., Probert, M.R. *The structure of a pentachromium(II) extended metal atom chain at 3 K: Cotton's conjecture proven* Dalton Trans., Advance Article, 2022
 20. Dehghan-Niri, R., Tsakoumis, N., Voronov, A., Holmen, A., Holmestad, R., Vullum, P.E., Borg, Ø., Rytter, E., Rønning, M., Walmsley, J.C. *Nanostructural Analysis of Co-Re/ γ -Al₂O₃ Fischer-Tropsch Catalyst by TEM and XRD* ChemCatChem, e202101931, 2022
 21. Djokić, V., Andričević, P., Kollár, M., Ciers, A., Arakcheeva, A., Vasiljević, M., Damjanović, D., Forró, L., Horváth, E., Ivšić, T. *Fast Lead-Free Humidity Sensor Based on Hybrid Halide Perovskite Crystals*, 12, 547, 2022
 22. Dutta, R., Thoma, H., Chernyshov, D., Nafradi, B., Masuda, T., Kriele, A., Hutanu, V. *Topological Analysis of the Experimental Electron Density in Multiferroic Antiferromagnet Ba₂MnGe₂O₇* IEEE Transac. on Magnetics, 58, 2, 2022
 23. Fatermans, J., Romolini, G., Altantzis, T., Hofkens, J., Roeyfaers, M.B.J., Bals, S., Van Aert, S. *Atomic-scale detection of individual lead clusters confined in Linde Type A zeolites* Nanoscale, 14, 9323-9330, 2022
 24. Frolov, K. V., O. A. Alekseeva, I. S. Lyubutin, V. Ksenofontov, E. S. Smirnova, V. L. Temerov, I. A. Gudim, and M. V. Lyubutina *Structural and Magnetic Phase Transitions in the Multiferroic HoFe₃(BO₃)₄ Observed by Mössbauer Spectroscopy and X-ray Diffraction* J. of Experimental and Theoretical Physics, 135, 698-707, 2022
 25. Fuller, C. A., Quintero-Castro, D. L., Bosak, A., Dyadkin, V., Chernyshov, D. *Correlated disorder and crystal structure of β -VOSO₄* Acta Cryst. B78, 2022
 26. Garcia-Ben, J., Garcia-Fernandez, A., Dafonte-Rodriguez, P., Degaldo-Ferreiro, I., Cappel, U.B., Castro-Garcia, S., Sanchez-Andujar, M., Bermudez-Garcia, J., Senaris-Rodriguez, M.A. *Narrowing the tolerance factor limits for hybrid organic-inorganic dicyanamide-perovskites* J. of Solid State Chem., 316, 123635, 2022
 27. Grigoryeva, N.A., Mistonov, A.A., Grigoriev, S.V. *Small-Angle Neutron Diffraction for Studying Ferromagnetic Inverse Opal-Like Structures* Crystallogr. Rep., 67, 93-117, 2022
 28. Grinderslev, J.B., Jensen, T.R. *Stabilization of ammonium borohydride in solid solutions of NH₄BH₄-MBH₄ (M = K, Rb, Cs)* Dalton Trans., 51, 17762-17771, 2022
 29. Guérin, L., Yoshida, T., Zatterin, E., Simonov, A., Chernyshov, D., Iguchi, H., Toudic, B., Takaishi, S., Yamashita, M. *Elucidating 2d charge-density-wave atomic structure in an mx-chain by the 3d-pair distribution function method* ChemPhysChem, e202100857, 2022

30. Hassen, S., Arfaoui, Y., Robeyns, K., Steenhaut, T., Filinchuk, Y., Klein, A., Chebbi, H. *Architecture of a dinuclear Co (II) complex based on 3-amino-1, 2, 4-triazole-5-carboxylic acid: molecular structure, thermal behavior, optical properties, and DFT calculations* J. of Coordination Chemistry 75, 908-924, 2022
31. Hofer, G., Schlüter, D., Weber, T. *Anatomy of a 2D Polymer Formation in the Single Crystal* Macromolecules, 2022
32. Kalantzopoulos, G.N., Gama, D.R., Pappas, D.K., Dovgaliuk, I., Olsbye, U., Beato, P., Lundegaard, L.F., Wragg, D.S., Svelle, S. *Real-time regeneration of a working zeolite monitored via operando X-ray diffraction and crystallographic imaging: how coke flees the MFI framework* Dalton Trans., Adv. Art, 2022
33. Kholina, Y., Dössegger, J., Weber, M.C., Simonov, A. *Metastable disordered phase in flash-frozen Prussian Blue analogues* Acta Cryst. B, 78, 3, 2022
34. Kiriukhina, G.V., Yakubovich, O.V., Dimitrova, O.V., Volkov, A.S. *New Microporous Copper Diphosphate Chloride in a Series of Homeotypic Compounds: Hydrothermal Synthesis, Crystal Structure, and Crystal Chemistry* Crystallogr. Rep., 67, 545–555, 2022
35. Kirsch, A., Bøjesen, E.D., Lefeld, N., Larsen, R., Mathiesen, J.K., Skjærvø, S.L., Pittkowsky, R.K., Sheptyakov, D., Jensen, K.M. *High-entropy oxides in the mullite-type structure* ChemRxiv, 2022
36. Klag, L., Sheppard, T.L., Grunwaldt, J.-D. *An Advanced Characterization Toolbox for Selective Olefin Oxidation Catalysts* ChemCatChem, 2022
37. Klimova, N., Snigireva, I., Snigirev, A., Yefanov, O. *Using diffraction losses of x-rays in a single crystal for determination of its lattice parameters as well as for monochromator calibration* J. Synchrotron Rad., 29, 369-376, 2022
38. Kochetygov, I., Justin, A., Asgari, M., Yang, S., Karve, V., Schertenleib, T., Stoian, D., Oveisi, E., Mensi, M., Queen, W.L. *3D vs. turbostratic: controlling metal-organic framework dimensionality via N-heterocyclic carbene chemistry* Chem. Sci., 13, 6418-6428, 2022
39. Kurdin, K.A., Kuznetsov, V.V., Sinitsyn, V.V., Galitskaya, E.A., Filatova, E.A., Belina, C.A., Stevenson, K.J. *Synthesis and characterization of Pt-HxMoO3 catalysts for CO-tolerant PEMFCs* Catal. Today, 388-389, 147-157, 2022
40. Kurlov, A., Stoian, D., Baghi Zadeh, A., Kountoupi, E., Deeva, E., Willinger, M., Abdala, P.M., Müller, C.R. *The structural evolution of Mo2C and Mo2C/SiO2 under dry reforming of methane conditions: morphology and support effects* ChemRxiv, 2022
41. Lätsch, L., Müller, I.B., Hassan, A., Perrone, B., Aghazada, S., Berkson, Z.J., Yakimov, A.V., De Baerdemaeker, T., Parvulescu, A.-N., Seidel, K., Teles, J.H., Copéret, C. *NMR Signatures and Electronic Structures of Ti-sites in Titanosilicalite-1 from solid-state 47/49Ti NMR Spectroscopy* ChemRxiv, 2022
42. Ma, G., Wang, L., Wang, X., Li, L., Ma, H. *CO oxidation over alumina-supported copper catalysts* Catalysts, 12, 1030, 2022
43. Magott, M., Ceglarska, M., Rams, M., Sieklucka, B., Pinkowicz, D. *Magnetic interactions controlled by light in the family of Fe(II)-M(IV) (M = Mo, W, Nb) hybrid organic-inorganic frameworks* Dalton Trans., 51, 8885-8892, 2022
44. Maity, A., Dutta, R., Sendtskyi, O., Ceretti, M., Lebranchu, A., Chernyshov, D., Bosak, A., Paulus, W. *Exploring Fast Room Temperature Oxygen Diffusion in Pr2NiO4+δ Stand-Alone Single-Crystalline Electrodes* Chem. Mater., 34, 414-421, 2022

45. Manceau, A., Simionovici, A., Findling, N., Glatzel, P., Detlefs, B., Wegorzewski, A.V., Mizell, K., Hein, J.R., Koschinsky, A. *Crystal Chemistry of Thallium in Marine Ferromanganese Deposits* ACS Earth Space Chem., 6, 5, 1269-1285, 2022
46. Mc Monagle, C.J., Michalchuk, A.A.L., Chernyshov, D. *FOX-7 high-energy-density material: thermal expansion and phase transitions revisited* Acta Cryst., B78, 91-95, 2022
47. Mc Monagle, C.J., Turner, G.F., Jones, I., Allan, D.R., Warren, M.R., Kamenev, K.V., Parsons, S., Wright, P.A., Moggach, S.A. *Pressure and guest-mediated pore shape modification in a small pore MOF to 1200 bar* Chem. Commun., 58, 11507-11510, 2022
48. Moury, R., Lodziana, Z., Remhof, A., Duchêne, L., Roedern, E., Gigante, A., Hagemann, H. *Study of the Temperature- and Pressure-Dependent Structural Properties of Alkali Hydrido-closo-borate Compounds* Inorg. Chem., 61, 13, 5224-5233, 2022
49. Naik, J.M., Bulfin, B., Triana, C.A., Stoian, D.C., Patzke, G.R. *Cation-deficient Ce-substituted perovskite oxides with dual-redox active sites for thermochemical applications* ACS Appl. Mater. Interfaces, 15, 1, 806-817
50. Nussbaum, S., Socie, E., Yao, L., Yum, J.-H., Moser, J.-E., Sivula, K. *Tuning Naphthalenediimide cations for incorporation into Ruddlesden-Popper-Tyde hybrid perovskites* Chem. Mater., 34, 3798-3805, 2022
51. Okatenko, V., Castilla-Amoros, L., Stoian, D.C., Vavra, J., Loiudice, A., Buonsanti, R. *The native oxide skin of liquid metal Ga nanoparticles prevents their rapid coalescence during electrocatalysis* J. Am. Chem. Soc., 144, 22, 10053-10063, 2022
52. Pages, A., Soh, J.-R., Fesharaki, M.J., Ronnow, H.M., Ahmadvand, H. *Revisiting the magnetic and crystal structure of multiferroic KNiPO₄* Cond. Mat., Adv. Art., 2022
53. Pankhurst, J.R., Castilla-Amoros, L., Stoian, D.C., Vavra, J., Mantella, V., Albertini, P.P., Buonsanti, R. *Copper phosphonate lamella intermediates control the shape of colloidal copper nanocrystals* J. Am. Chem. Soc., 144, 27, 12261-12271, 2022
54. Pedersen, V.H., Blichfeld, A.B., Bakken, K., Chernyshov, D., Grande, T., Einarsrud, M.-A. *Crystallization and texturing of Sr_xBa_{1-x}Nb₂O₆ thin films prepared by aqueous solution deposition - An in situ X-ray diffraction study* Cryst. Growth Des., 22, 10, 5912-5922, 2022
55. Pereniguez, R., Ferri, D. *In Situ Xrd and Operando Xrd-Xas Study of the Self-Regenerative Behaviour of LaCo_{0.8}Cu_{0.2}O₃ Perovskite for Preferential Oxidation of Co* SSRN, 4186992, 2022
56. Pittkowski, R., Clausen, C. M., Chen, Q., Stoian, D., van Beek, W., Bucher, J., Welten, R.L., Schlegel, N., Mathiesen, J.K., Nielsen, T.M., Rosenkranz, A.W., Bojesen, E.D., Rossmeisl, J., Jensen, K.M.O., Arenz, M. *High entropy alloy nanoparticle formation at low temperatures* ChemRxiv, 2022
57. Prodinge, S., Kvande, K., Arstad, B., Borfecchia, E., Beato, P., Svelle, S. *Synthesis-structure-activity relationship in Cu-MOR for partial methane oxidation: Al Siting via inorganic structure-directing agents* ACS Catal., 12, 4, 2166-2177, 2022
58. Reberc, M., Mazaj, M., Stare, J., Pockaj, M., Mali, G., Li, X., Filinchuk, Y., Cerny, R., Meden, A. *Trinuclear magnesium imidazolate borohydride complex* Inorg. Chem., 61, 32, 12708-12718, 2022
59. Saedy, S., Newton, M.A., Zabilskiy, M., Hee Lee, J., Krumeich, F., Ranocchiari, M., van Bokhoven, J.A. *Copper-zinc oxide interface as a methanol-selective structure in Cu-ZnO catalyst during catalytic hydrogenation of carbon dioxide to methanol* Catal. Sci. Technol., 12, 2703-2716, 2022
60. Shvets, P.V., Prokopovich, P.A., Dolgoborodov, A.I., Usoltsev, O.A., Skorynina, A.A., Kozyr, E.G., Shapovalov, V.V., Guda, A.A., Bugaev, A.L., Naranov, E.R., Gorbunov, D.N., Janssens, K., De Vos, D.E.,

- Trigub, A.L., Fonda, E., Leshchinsky, M.B., Zagackij, V.R., Soldatov, A.V., Goikhman, A.Y. *In Situ X-ray Absorption Spectroscopy Cells for High Pressure Homogeneous Catalysis Catalysts*, 12, 1264, 2022
61. Sminorva, E.S., Alekseeva, O.A., Dudka, A.P., Sorokin, T.A., Khmelenin, D.N., Yapaskurt, V.O., Lyubutina, M.V., Frolov, K.V., Lyubutin, I.S., Gudim, I.A. *Crystal structure, absolute configuration and characteristic temperatures of SmFe₃(BO₃)₄ in the temperature range 11-400 K* Acta. Cryst., B78, 546-556, 2022
62. Sørby, M.H., Martinsen, F., Karazhanov, S.Z., Hauback, B.C., Marstein, E.S. *On the Crystal Chemistry of Photochromic Yttrium Oxyhydride* Energies, 15, 1903, 2022
63. Steele, J.A., Braeckvelt, T., Prakasam, V., Degutis, G., Yuan, H., Jin, H., Solano, E., Puech, P., Basak, S., Pintor-Monroy, M.I., Van Gorp, H., Fleury, G., Yang, R.X., Lin, Z., Huang, H., Debroye, E., Chernyshov, D., Chen, B., Wei, M., Hou, Y., Gehlhaar, R., Genoe, J., De Feyter, S., Rogge, S.M.J., Walsh, A., Sargent, E.H., Yang, P., Hofkens, J., Van Speybroeck, V., Roeloffs, M.B.J. *An embedded interfacial network stabilizes inorganic CsPbI₃ perovskite thin films* Nat Commun, 13, 7513, 2022
64. Stehle, M., Gaur, A., Weber, S., Sheppard, T.L., Thomann, M., Fischer, A., Grunwaldt, J.-D. *Complementary operando insights into the activation of multicomponent selective propylene oxidation catalysts* J. of Catalysis, 408, 339-355, 2022
65. Strandbakke, R., Wragg, D.S., Sørby, M.H., Guzik, M.N., Gunnæs, A.E., Szpunar, I., Wachowski, S.L., Balaguer, M., Carvalho, P.A., Mielewczyk-Gryn, A., Serra, J.M., Norby, T. *Structural properties of mixed conductor Ba_{1-x}Gd_{1-y}La_{x+y}Co₂O_{6-δ}* Dalton Trans., 51,18667-18677, 2022
66. Tafjord, J., Regli, S.K., Dugulan, A.I., Ronning, M., Rytter, E., Holmen, A., Myrstad, R., Yang, J. *Influence of temperature during pyrolysis of fe-alginate: Unraveling the pathway towards highly active Fe/C catalysts* Applied Catalysis A, Gen. 644, 118834, 2022
67. Tsoukalou, A., Serykh, A.I., Willinger, E., Kierzkowska, A., Abdala, P.M., Fedorov, A., Müller, C.R. *Hydrogen dissociation sites on indium-based ZrO₂-supported catalysts for hydrogenation of CO₂ to methanol* Catal. Today, 387, 38-46, 2022
68. Valle, E., Duyar, M.S., Snider, J.L., Regli, S.K., Rønning, M., Gallo, A., Jaramillo, T.F. *In Situ Studies of the Formation of MoP Catalysts and Their Structure under Reaction Conditions for Higher Alcohol Synthesis: The Role of Promoters and Mesoporous Supports* J. Phys. Chem. C, 126, 12, 5575-5583, 2022
69. Van der Heggen, D., Zilenaite, R., Ezerskyte, E., Fritz, V., Korthout, K., Vanderberghe, D., De Grave, J., Garrevoet, J., Vincze, L., Poelman, D., Joos, J.J., Smet, P.F. *A standalone, battery-free light dosimeter for ultraviolet to infrared light* Adv. Funct. Materials, 32, 2109635, 2022
70. Walker, J., Marshall, K.P., Salgado-Beceiro, J., Williamson, B.A.D., Londal, N.S., Castro-Garcia, S., Sanchez Andujar, M., Selbach, S.M., Chernyshov, D., Einarsrud, M.-A. *Mesophase Transitions in [(C₂H₅)₄N][FeBrCl₃] and [(CH₃)₄N][FeBrCl₃] Ferroic Plastic Crystals* Chem. Mater., 34, 2585-2598, 2022
71. Wang, X., Liu, Z., Li, G., Jiang, G., Zhao, Y., Li, L., Li, K., Liang, G., Gao, S., Xi, H., Li, S., Zou, R. *High-efficiency capture of ammonia using hierarchically porous Zr-MOF nanoarchitectures under ambient conditions: Thermodynamics, kinetics, and mechanisms* Chem. Eng. Journal, 440, 135764, 2022
72. Yakubovich, O.V., Shvanskaya, L.V., Kiriukhina, G.V., Dimitrova, O.V., Volkov, A.S., Volkova, O.S., Vasiliev, A.N. *Sawtooth chains self-assembled from clusters of MnO₆ octahedra within the silicate framework of K₃Mn₄Si₁₀O_{24.33}(H₂O,OH)₃/V,B* CrystEngComm., 24, 6964-6973, 2022
73. Yoshida, T., Takaishi, S., Guérin, L., Kojima, T., Ohtsu, H., Kawano, M., Miyamoto, T., Okamoto, H., Kato, K., Takata, M., Hosomi, Y., Yoshida, S., Shigekawa, H., Tanaka, H., Kuroda, S.-I., Iguchi, H.,

- Breedlove, B.K., Li, Z.-Y., Yamashita, M. *Hydrogen Bonding Propagated Phase Separation in Quasi-Epitaxial Single Crystals: A Pd-Br Molecular Insulator* Inorg. Chem., 61 (35), 14067-14074, 2022
74. Yüzbaşı, N.S., Armutlulu, A., Huthwelker, T., Abdala, P.M., Müller, C.R. *Na- β -Al₂O₃ stabilized Fe₂O₃ oxygen carriers for chemical looping water splitting: correlating structure with redox stability* J. Mater. Chem. A, Advance Article, 2022
75. Zhao, Y., Dongfang, N., Triana, C.A., Huang, C., Erni, R., Wan, W., Li, J., Stoian, D., Pan, L., Zhang, P., Lan, J., Iannuzzi, M., Patzke, G.R. *Dynamics and control of active sites in hierarchically nanostructured cobalt phosphide/chalcogenide-based electrocatalysts for water splitting* Energy Environ. Sci, Advanced Article, 2022
76. Zhao, Y., Wan, W., Dongfang, N., Triana, C.A., Douls, L., Huang, C., Erni, R., Iannuzzi, M., Patzke, G.R. *Optimized NiFe-based coordination polymer catalysts: Sulfur-tuning and operando monitoring of water oxidation* ACS Nano, 16, 9, 15318-15327, 2022
77. Zimmerli, N.K., Müller, C.R., Abdala, P.M. *Deciphering the structure of heterogeneous catalysts across scales using pair distribution function analysis* Trends in Chem., 4, 9, 807-821, 2022

SNBL software outreach

SNBL provides for many years now open source software to its users and to a broader scientific community. It can be downloaded on the following page <https://soft.snbl.eu/>

There are various software suits available for:

1. beamline control
2. various types of data conversion
3. fast on-line powder integration
4. visualisation and frequency analysis for modulation-enhanced powder diffraction
5. refinement of absolute structure
6. Inspection and geometric Ewald sphere corrections of GISAXS and GIWAXS data
7. Sequential refinement of multiple single crystal datasets with CrysAlis and shelx

The software is described in the following paper: J. Synchrotron Rad. (2016). 23, 825-829 which has received 300 citations to date. It appears from the 300 citations that SNBL software is installed and used at at least 8 beamlines spread over three synchrotrons. BM01, BM31, BM14, BM26, BM20 and ID28 at the ESRF. Materials Science beamline at Swiss light source and NCD-SWEET at ALBA.

Summary of the works

BM01 installation of SAXS detector lift

On BM01 the major job to be done was the construction and installation of a second detector support for SAXS. The detector is now installed and integrated in the data acquisition software.

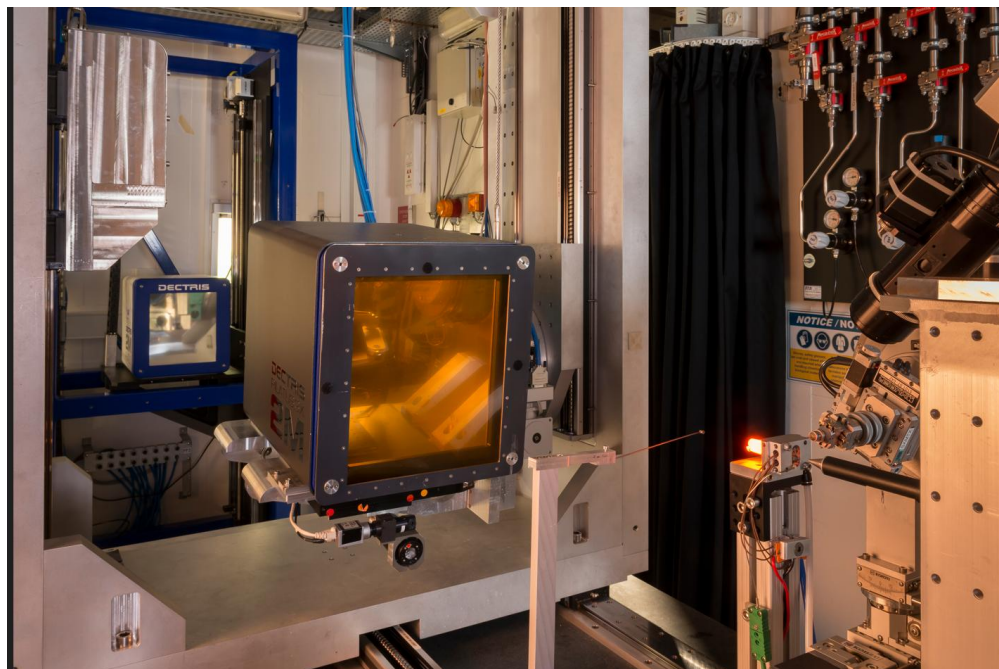


Figure 1. Two detectors installed on BM01

BM31 installation of new end-station

The works on BM31 are part of a project funded by the Swiss National Science Foundation (SNSF) and the Research Council of Norway (RCN). The project is called: *Enhanced combination of synchrotron diffraction and spectroscopy for studying materials and processes focussed on sustainable technologies and environmental issues* and spread over several years.

The scientific justification and aims are as follows. The increasingly rapid transition to sustainable technologies relies on the development of innovative materials utilizing an in-depth understanding of the interplay between a material's structure and its macroscopic properties (e.g. catalytic activity). In this context, X-ray-based methods that allow to probe complex materials' structures at different lengths and time scales are key to obtaining fundamental insight paving the way to the rational design of novel materials. Hence, the goal of this project was the design and implementation of a combined X-ray powder diffraction (XRD), pair distribution function (PDF) analysis and X-ray absorption spectroscopy (XAS) set up at the BM31 station of the Swiss Norwegian Beam Lines (SNBL) at the European Synchrotron Radiation Facility (ESRF). The combined XRD-PDF-XAS station allows the acquisition of complementary information, covering the length-scales from short to mid-range atomic arrangements viz. $\sim 1 \text{ \AA}$ to several nm by PDF, the average structure by XRD, as well as the electronic state, and geometry around the elements of interest by XAS. XRD refers to the conventional analysis

of powder diffraction data in reciprocal space (Bragg peaks) and PDF to the analysis of (high energy) total scattering data that includes both Bragg peaks and diffuse scattering. To our best knowledge, with this upgrade, BM31 became globally a unique facility for the performance of XAS-XRD-PDF experiments.

The implementation of such a combination of techniques requires a setup that is capable of exchanging between XAS, XRD and PDF configurations in a fast and reproducible manner, without compromising the quality of each technique.

To achieve the goal of combining XRD-PDF-XAS measurements in a single setup, a new end-station for the beamline was custom designed by the project team in 2021. All individual components were also ordered in 2021. In the spring of 2022 the new end-station was assembled and tested off-line. A boundary condition for the implementation of the project was the minimal interruption of ongoing user experiments. This constraint imposed a major challenge, limiting the installation period to the summer shutdown of the synchrotron (i.e. July-August 2022). The new setup (see Figure 2 below) comprised the mounting of a marble support, 32 motors and 18 detectors that were all individually tuned, tested and interfaced with the relevant software. In addition, the existing infrastructure of the gas supplies had to be rerouted.

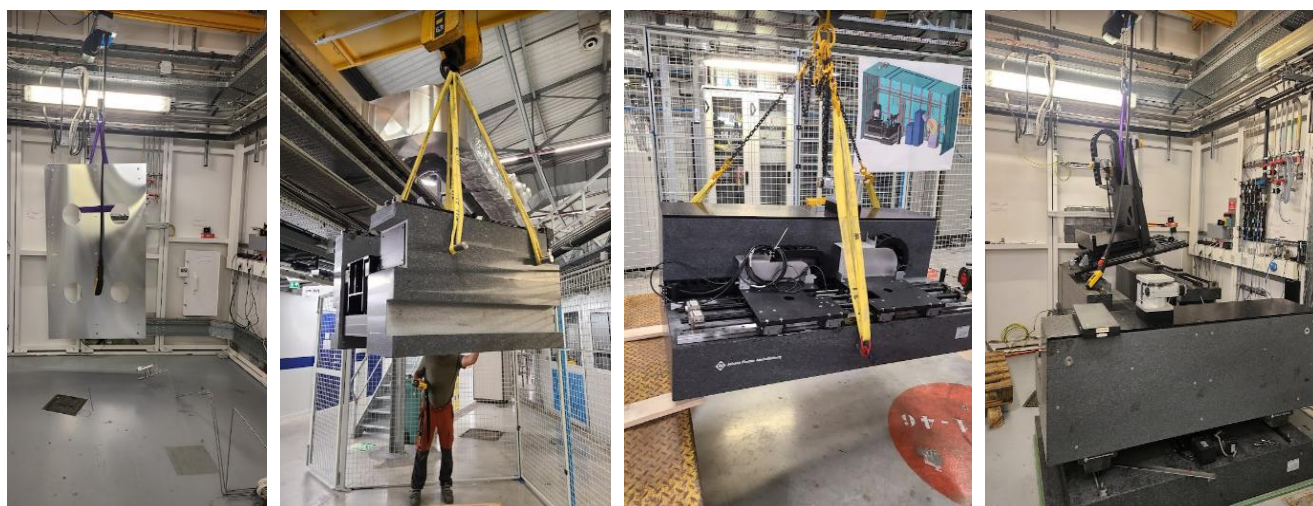


Figure 2. Photographs showing the installation of the new end station, i.e. from the dismantling of the former equipment to mounting the new setup.

Commissioning of the CdTe 2M detector

The PILATUS3 X CdTe 2M detector provided by DECTRIS Ltd. (Switzerland) is a high-end photon-counting detector, detecting efficiently photons up to 100 keV. This detector was the core of the project, allowing for the effective acquisition of time-resolved, high-energy XRD-PDF data. The detector consists of 2 million, micronmeter-sized, individual single photon counting elements. Acceptance tests of the new detector were performed by SNBL staff in collaboration with specialists from the ESRF detector laboratory. These acceptance tests included a verification of its spatial resolution, count rate, dark images, defective pixels, flat-field, Poisson statistics, maximum frame rate, triggering modes, initial stabilization, long-term stability under irradiation, afterglow, global count rate or geometrical distortions. After the successful completion of the acceptance tests of the PILATUS 3X, 2M CdTe detector all new elements of the set-up were combined the experimental hutch (See Figure 3 below). The last step of the commissioning phase was to interface and control all equipment with the relevant software tools. The IT required to acquire combined XAS-XRD-PDF data was implemented by SNBL

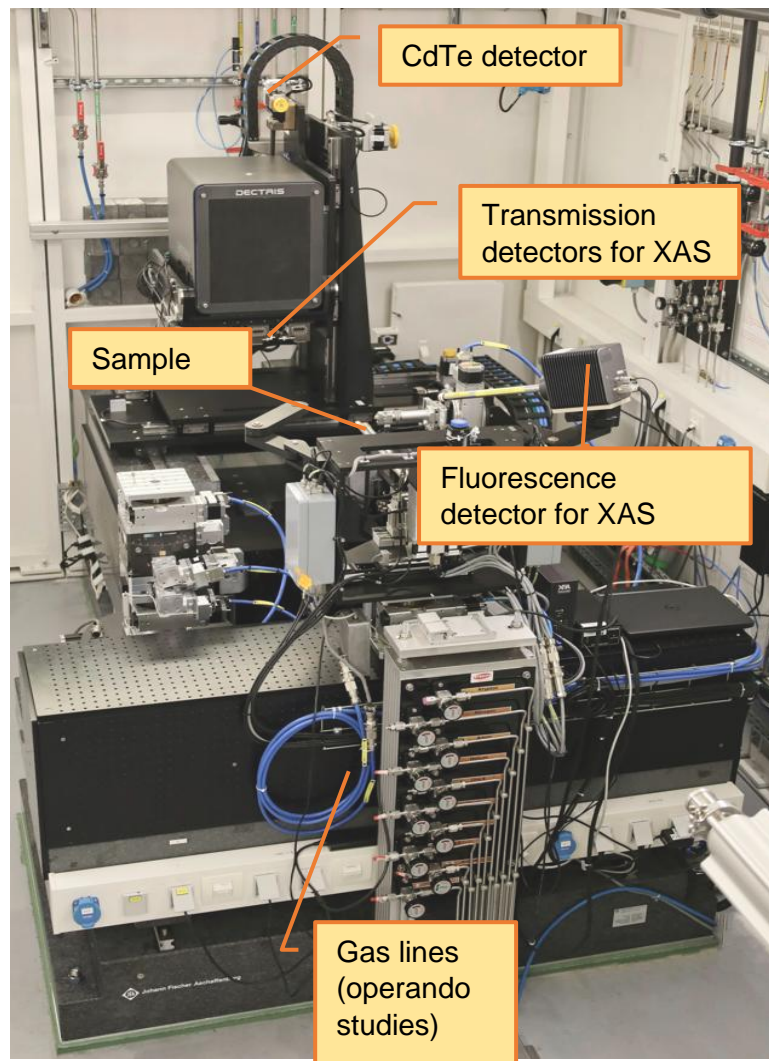


Figure 3: Photograph of the sample measurements stage located in the new end-station.

staff; furthermore, the project benefited from data processing and analysis software suites developed prior by SNBL staff. Currently, further software capabilities are being developed to assist complex user experiments.

Benchmarking of X-ray total scattering and XAS data with the new endstation

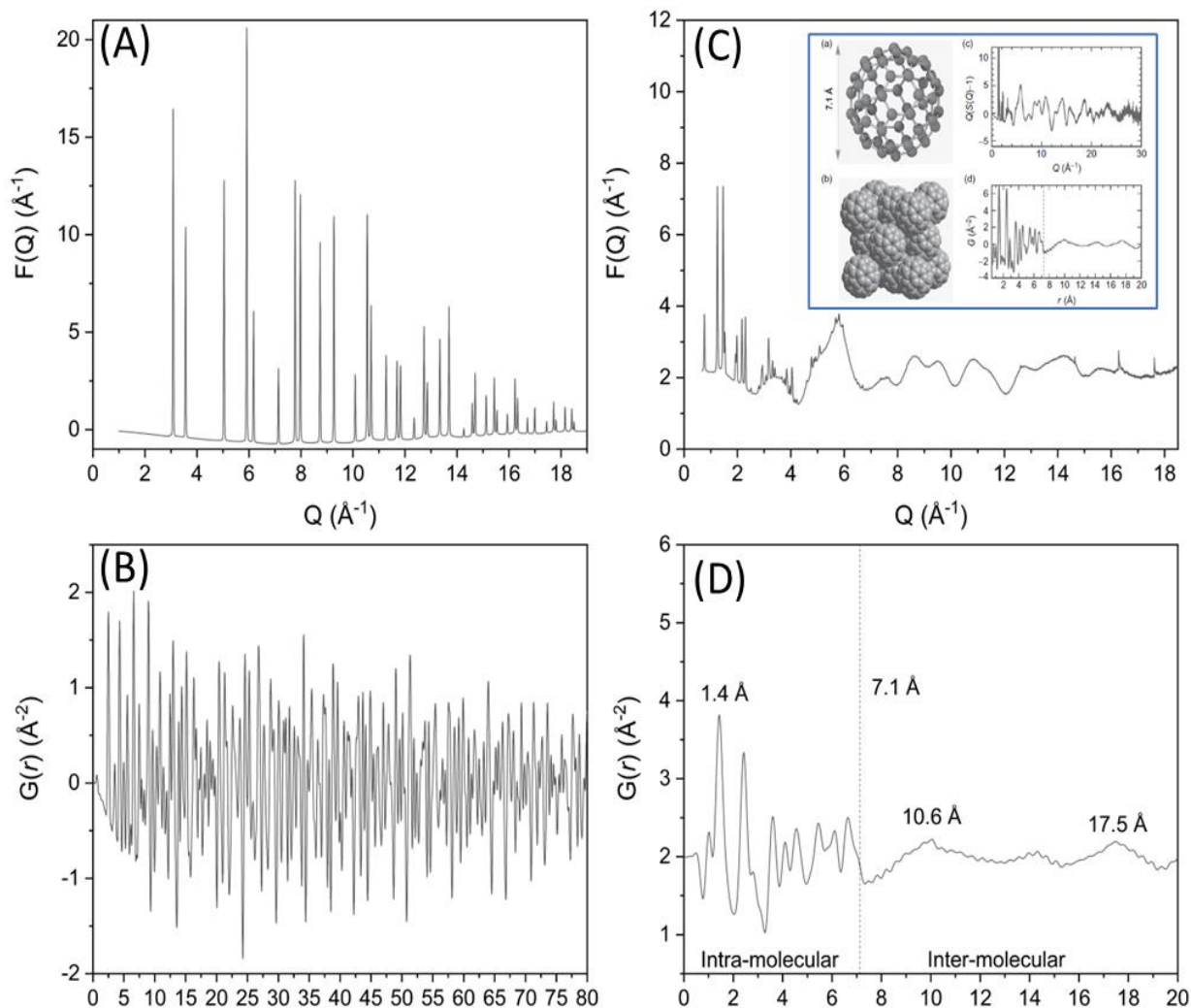


Figure 1: (a) $F(Q)$ and (b) $G(r)$ of Ni (powder) and (c) $F(Q)$ and (d) $G(r)$ of C60. The inset in (C) shows the atomic structure of C60 with the respective $Q(S)$ and $G(r)$ data as reproduced from reference ⁵.

After the successful commissioning of the new end station with the new PILATUS 3X 2M CdTe detector, a series of tests were performed using X-rays (synchrotron operating in a low intensity mode, 4-bunch). XAS measurements followed by total scattering (XRD-PDF) experiments were performed. The XAS performance was tested on different energy ranges, using standard foils. XAS data of high quality were obtained. Importantly, the XAS data could be collected in an automatic and rapid manner at very different energy ranges; e.g., between Ir (11.5 keV) and Ag (25.5 keV) K-edges. Such capabilities are important for in situ studies at multiple edges (e.g., to study high entropy alloys in situ). Next, the new total scattering capabilities were evaluated, by using two benchmark materials (Ni and C60 powders as benchmarks of a strong and a weak scatterer material, respectively). The data collection of the total scattering data for PDF analysis was

performed with a monochromatic beam set at a wavelength of 0.323 Å using the new acquired PILATUS3 X CdTe 2M detector (distance sample-detector of ca. 19 cm, $Q_{\max}=19 \text{ \AA}^{-1}$). The powders were placed inside glass capillaries of 0.5 mm in diameter. Each scattering image was recorded with a 36 s exposure time. For each measurement, 3 (for Ni) or 20 (for C60) images were averaged. An empty capillary was measured under the same conditions. The normalized scattering functions, $F(Q)$, and the pair distribution functions, $G(r)$ were calculated from the total scattering data using PDFgetX3 V. 2.2.1, using data obtained from the empty capillary as background.^{2,3} In Figure 4 the data collected from the highly crystalline Ni powder is plotted. The PDF of Ni has been documented in literature and can thus be used as a benchmark.⁴ Our collected data agree very well with literature data showing identical features. The Q resolution of the acquired data is excellent, allowing us in the future to access medium-range distances, 10-100 Å, which is important, for instance, to determine nanoparticle size and shape. The data collected on C60 is plotted in Figure 4c,d and it demonstrates the feasibility of the new set-up to perform PDF analysis on a very weakly scattering material. The data displayed in Figure 4d clearly shows a transition at 7.1 Å between intra-ball C-C correlations and very weak inter ball correlations above 7.1 Å (in addition to the local structural features of C60 with the minimum distance at ca. 1.4 Å).⁵ As these test were performed in low intensity mode of the synchrotron the time resolution is not representative of the final performance.

Finally, we critically assessed the functionality of the new set-up by performing a combined XAS – XRD – PDF experiment on a catalyst. The material consists of very small (ca. 2 nm diameter) nanoparticles of Ni and Ga (3 wt. % metal loading) supported onto a SiO₂ carrier. To extract information about the supported nanoparticles

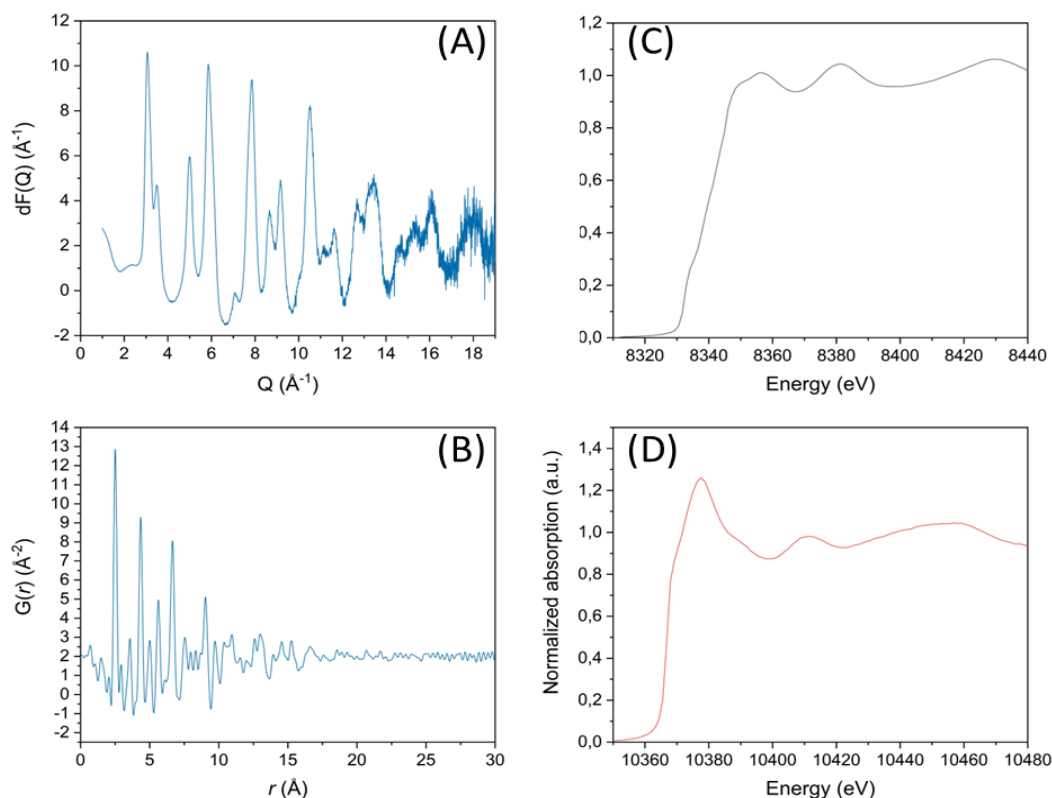


Figure 5. (a) Differential $F(Q)$, (b) $G(r)$, (c) XANES at the Ni K-edge (and (d) Ga K-edge data of a Ni_xGa_y/SiO₂ catalyst.

we performed a differential d-PDF analysis by subtracting the PDF data of the SiO₂ support. The reciprocal space data, the d-PDF analysis together with XANES at the Ni and Ga K-edges are presented in Figure 5. This experiment demonstrated very convincingly the exciting new functionalities the new set-up is able to provide, i.e. the acquisition of combined XRD-PDF-XAS data on a complex (real) catalysts system.

Conclusions and outlook

To summarize, the project achieved all of its goals, i.e. adding the new functionality to SNBL's portfolio of acquiring combined XAS-XRD-PDF experiments. The first XAS-XRD-PDF dataset on a complex catalyst was successfully collected. The SNBL user program started with the new setup as planned. Current experiments on BM31 are being performed using the newly enveloped setup and importantly under in situ and operando conditions (via a proposal-based scheme). We expect that in the years to come, this setup will allow the detailed study of various materials for a wide range of applications, including heterogeneous catalysis, CO₂ capture, gas separation and batteries.

References

1. Abdala, P. M.; Safonova, O. V.; Wiker, G.; van Beek, W.; Emerich, H.; van Bokhoven, J. A.; Sa, J.; Szlachetko, J.; Nachttegaal, M. *Chimia* **2012**, 66, (9), 699-705.
2. Zimmerli, N. K.; Müller, C. R.; Abdala, P. M. *Trends in Chemistry* **2022**, 4, (9), 807-821.
3. Chapter 5 Data collection and analysis. In *Pergamon Materials Series*, Egami, T.; Billinge, S. J. L., Eds. Pergamon: 2003; Vol. 7, pp 137-216.
4. Billinge, S. J. L. *Philosophical Transactions of the Royal Society A: Mathematical, Physical and Engineering Sciences* **2019**, 377, (2147), 20180413.
5. Proffen, T.; Billinge, S. J. L.; Egami, T.; Louca, D. *Zeitschrift für Kristallographie - Crystalline Materials* **2003**, 218, (2), 132-143.
6. van Beek, W.; Emerich, H.; Chernyshov, D.; Dyadkin, V.; Wiker, G.; Dmitriev, V. *Acta Crystallographica Section A* **2019**, 75, (a2), e677.